Synthesis and Photophysical Characterization of Unsymmetrical Squaraine Dyes for Dye-Sensitized Solar Cells utilizing Cobalt Electrolytes

著者	Pradhan Anusha, Saikiran Maryala, Kapil Gaurav, Hayase Shuzi, Pandey Shyam Sudhir
journal or publication title	ACS Applied Energy Materials
volume	1
number	9
page range	4545-4553
year	2018-08-24
URL	http://hdl.handle.net/10228/00007348

doi: info:doi/10.1021/acsaem.8b00653

Synthesis and Photophysical Characterization of Unsymmetrical Squaraine Dyes for Dye-Sensitized Solar Cells utilizing Cobalt Electrolytes

Anusha Pradhan*, Maryala Sai Kiran, Gaurav Kapil, Shuzi Hayase, Shyam S. Pandey*
Graduate School of LSSE, Kyushu Institute of Technology, 2-4 Hibikino, Wakamatsu, Kitakyushu, 808-0196, Fukuoka, Japan
*Email: ansupradhan9@gmail.com; shyam@life.kyutech.ac.jp

Abstract

Development of novel near infra-red (NIR) dyes compatible with cobalt complex based redox shuttles for their utilization, as sensitizer is inevitable for the fabrication of high efficiency dye-sensitized solar cells (DSSCs). A Series of newly designed unsymmetrical squaraine dyes as model of NIR sensitizer were synthesized and characterized for their application as far-red sensitizers of DSSCs utilizing $Co(bpy)^{2+/3+}$ redox electrolyte. It was shown that logical molecular design led to not only energetic tunability of the sensitizers but also possibility of good photon far-red photon harvesting up to 750 nm. One of the newly designed sensitizers SQ-110 bearing two long alkyl substituents in combination with electron donating methoxy group directly linked to the aromatic ring was par excellent in terms of its photoconversion efficiency amongst the dyes utilized in this work. DSSC fabricated using SQ-110 as sensitizer and $Co(bpy)^{2+/3+}$ redox electrolyte furnished a photoconversion efficiency of 1.98 % along with good photon harvesting mainly in the far-red wavelength region. It was further demonstrated that dye molecular structure plays rather more prominent role than their energetics in controlling the overall device performance of the DSSCs.

1. Introduction

Dye-sensitized solar cells (DSSCs) are one of the promising candidates amongst next generation solar cells in terms of their ease of fabrication, cheap raw materials and vivid color. After the pioneering work by Reagan and Gratzel in 1991, DSSC has been emerged as one of the alternatives to the costly silicon solar cells and expected to pave the way for the cost-effective solar energy harvesting [1]. DSSCs consist of a photoanode, which is typically TiO_2 semiconductor covered with monolayer of dye adsorbed on to it. The adsorbed dyes on the mesoporous TiO_2 nanoparticles are involved in the photon harvesting after their photoexcitation followed by electron injection in to the conduction band of TiO_2. Therefore, sensitizing dyes play the crucial role in DSSC working cycle being actual photon harvester and deserves to be considered as the heart of the DSSCs [2]. In principle after the photoexcitation, the dye must be regenerated by the ionic electrolyte faster than recombination from injected electrons in TiO_2, or in other words, the forward injection should be more efficient than the back electron transfer, which takes place at photoanode/electrolyte the interfaces [3]. At this point, the dye design and electrolyte selection becomes an important step to obtain efficiently working DSSCs [4]. DSSCs with an impressive photoconversion efficiency (PCE) > 12% have been reported utilizing porphyrin dyes in spite of having photon harvesting mainly in the visible region of solar spectrum [5, 6]. A perusal of the electronic absorption spectra and the efficient photon harvesting by a number of the efficient visible light absorbing sensitizers indicates the need for design and development of novel sensitizers absorbing in near infra-red (NIR) wavelength region for further enhancement in the PCE [7, 8,9].

Most commonly used iodine based electrolytes are still one of the preferred choices amongst electrolytes, which functions well with a variety of sensitizing dyes in the DSSC research. However, complex redox mechanism, intense color and corrosiveness of this class of

electrolytes are issues of concern and led to the proposal as well as implementation of alternate redox shuttles [10]. In this context, one electron redox shuttles based on metalorganic Co(II)/Co(III) complexes have been emerged as an obvious choice due to their simpler outer sphere electron transfer kinetics and easy dye regeneration process, reducing the correlated loss of open-circuit voltage [11]. However, cobalt complex based redox mediators are more prone to recombination owing to their relatively bulky size and slow ionic diffusion [12]. Unlike iodine-based electrolytes, cobalt electrolytes bear positive surface charge exhibiting an obvious attractive interaction with the negatively charged TiO_2, which demands for the strict surface passivation. This is the reason why many of the sensitizers working well with iodine based electrolyte exhibit hampered photon harvesting when the same is being employed with cobalt electrolyte [11]. It has been found that sensitizing dyes bearing multiple and long alkyl chains as substituent in main dye framework are capable of inhibiting back electron transfer from the TiO_2 to the redox shuttle and function well with the cobalt redox mediators [13].

Various dyes reported till date as sensitizers for DSSCs compatible with cobalt electrolyte generally bear multiple and long alkyl chains but their photon harvesting < 750 nm still invokes a huge demand for the design and development of NIR dyes compatible with cobalt redox mediators [14-15]. In fact, we have reported DSSCs utilizing squaraine dyes as sensitizer and iodine/cobalt based redox electrolytes. It was found that same dyes, which exhibited good far-red photon harvesting and efficiency with I^-/I_3^- electrolyte ended with very poor efficiency (0.2-0.3 %) with cobalt electrolyte [16]. Since cobalt based redox electrolytes have relatively deeper redox energy level as compared to commonly used iodine based electrolytes, care must be taken for controlling the energetics of the newly designed dyes under investigation. Recently we have demonstrated about the need for minimum driving force of

0.12 eV for the dye regeneration using model squaraine dyes and iodine based redox electrolyte [17].

In this work, we would like to report about the design of novel blue colored dyes possessing an intense and sharp light absorption along with the photon harvesting mainly in the far-red region. Our design was based on the introduction of long alkyl chain dye molecular structure required to work with the cobalt-based redox shuttle along with control of their energetics in terms of energy of their highest occupied molecular orbital (HOMO) and lowest unoccupied molecular orbital (LUOM) with respect to energy levels of cobalt bipyridyl redox mediator and conduction band (CB) of TiO2, respectively. Maintaining a finite driving force for dye regeneration and electron injection along with surface passivation by compact TiO2 layer, far-red sensitive unsymmetrical squaraine dyes with molecular structure shown in the Fig. 1 were synthesized and subjected to their photophysical characterization along with application as sensitizer for DSSCs.

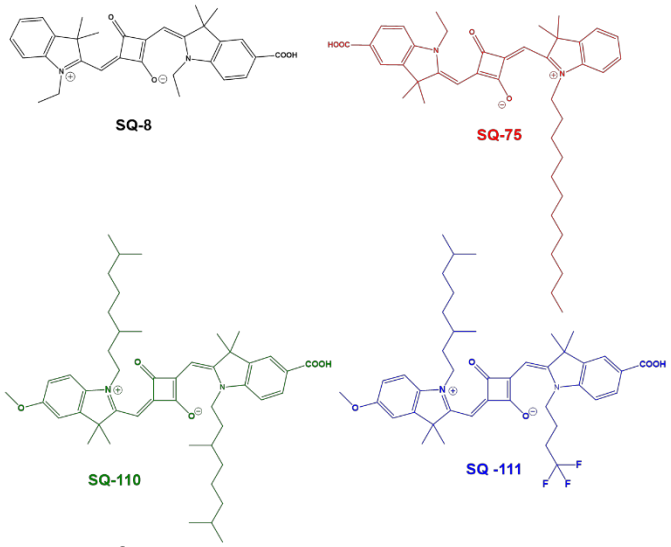

Figure 1. Molecular Structure of the unsymmetrical Squaraine dyes utilized in the present work.

2. Experimental

2.1 MATERIALS AND METHODS

All of the chemicals were of analytical grade and used without further purification. Progress of the reaction for synthesis was monitored on TLC Silica gel 60G F_{25} as well as high-performance liquid chromatography (HPLC). Dye intermediates as well as dyes were then subjected to MALDI-TOF in the positive ion mode using α-CHCA matrix to confirm their respective mass. Finally, the synthesized dyes were then again subjected to fast ion bombardment (FAB)-mass spectrometry in the positive ion-monitoring mode. Nuclear magnetic resonance (NMR) spectrum (JEOL, 500 MHz) of the dyes was conducted by dissolving them in $CDCl_3$/DMSO-d_6 for the structural verification. Electronic absorption spectra of the sensitizers in solution (ethanol) as well as solid-state on thin transparent TiO_2 film was taken with the help of UV-Visible-NIR spectrometer (JASCO model V550). HOMO energy level of the sensitizing dyes was determined using photoelectron yield spectroscopy (Bunko Keiki, model KV-205 HK, Japan). Subsequently, LUMO energy level was estimated by adding the optical energy band gap (Eg), estimated from the relation 1240/λ, where λ corresponds to the onset wavelength of the absorption spectra in the solid state. The Solar simulator (CEP-2000 Bunko Keiki Co. Ltd, Japan) equipped with a xenon lamp (Bunko Keiki BSO-X150LC) employing a light source of a simulated solar intensity of 100 mW/cm^2 was used to measure the photovoltaic characteristics of the DSSCs maintaining the working area of 0.2025 cm^2 precisely with a black metal mask.

DSSCs comprised of the dye-adsorbed mesoporous TiO_2 coated on fluorine-doped tin oxide (FTO) conducting glass as photoanode, $Co(bpy)^{2+/3+}$ redox electrolyte and platinum sputtered on to FTO (60 nm) as photocathode. The photoanode preparations was started with the washing of the 2 × 1 cm^2 FTO glass substrates with detergent, distilled water, acetone and isopropyl alcohol subsequently under sonication for 15 minutes each followed by ozone plasma

treatment. Cleaned FTO substrates were subjected to surface treatment by dipping in the 40mM solution of $TiCl_4$ for 30 mins at 70^0C and then sintered at 450^0C for 30 mins. The $TiCl_4$ treated FTO substrates were then screen printed with TiO_2 paste (DS/P Solaronix) to afford the mesoporous TiO_2 having thickness of about 7 μm. This mesoporous TiO_2 surface was again subjected to $TiCl_4$ treatment as described above. The mesoporous TiO_2 coated FTOs were then dipped in 0.2 mM solution of the respective dyes along with 4 mM Chenodeoxycholic acid as coadsorber in anhydrous ethanol for 4 hours at room temperature. The photoanode and the photocathode were then affixed using a 25 μm surlyn spacer at 110^0C. The electrolyte was then injected through the aperture between the spacer and the finally sealed with a UV resin. The electrolyte comprised of 0.22M $[Co(bpy)_3(PF_6)_2]$, 0.033 M of $[Co(bpy)_3(PF_6)_2]$, 0.2 M of tert.-butyl-pyridine and 0.1 M $LiClO_4$ in acetonitrile.

2.2 SYNTHESIS OF UNSYMMETRICAL SQUARAINE DYES

Unsymmetrical squaraine dyes SQ 8 and SQ 75 were and dye intermediate 1,1,1-Trifluorobutyl-5-carboxy-2,3,3-trimethyl-indolium iodide (6) were synthesized as per our earlier publications [18, 19]. Unsymmetrical squaraine dyes SQ-110 and SQ-111 along with their respective intermediates were synthesized as per the synthetic scheme shown in Fig. 2.

2.2.1 SYNTHESIS OF 5-METHOXY-2,3,3-TRIMETHYL 3H –INDOLIUM IODIDE [1]

3-methyl-2-butanone (10.9 g, 125 mmol) was added to a round bottom flask containing 50 mmol of 4-methoxy phenyl hydrazine hydrochloride (8.6 g) in 80 mL of glacial acetic acid. The mixture was refluxed for 18 hours. The solvent was evaporated under reduced pressure and the concentrated compound was extracted with chloroform. Chloroform was evaporated and the crude compound obtained was subjected to flash column chromatography in Ethyl acetate/ Hexane system (1:1) as the eluting solvent leading targeted compound as a brown viscous liquid in 94% yield. The synthesis of the titled compound was justified by the MALDI-

TOF measurement mass (measured m/z: 248.0 $[M+2]^+$; calculated m/z: 246.19) confirms the synthesis of this intermediate.

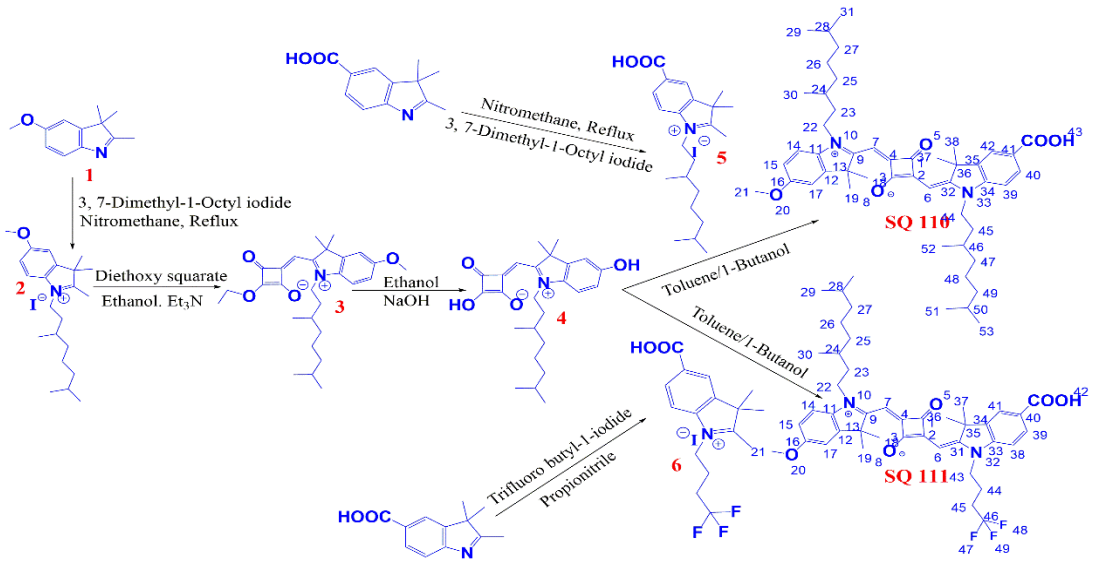

Figure 2. Scheme for the synthesis of unsymmetrical squaraine dyes SQ-110 and SQ-111.

2.2.2 Synthesis of 5-Methoxy-2,3,3-Trimethyl-1-Dimethyl-Octyl-Indolium Iodide [2]

In a round bottom flask, fitted with a condenser, 3.6 g (18.4 mmol) of compound (1) and 1.5 equivalents (7.4 gm; 27.6 mmol) of 3,7-Dimethyl-1-Octyl-Iodide were dissolved in 50 mL nitromethane and refluxed for 48 hours. After the completion of the reaction as confirmed by TLC, the solvent was evaporated completely and the compound was washed with ample diethyl ether to obtain the title product as an orange viscous liquid in 67% yield and >98 % HPLC purity. [FAB-MS Calculated, 330.28 and measured, 331.57 $(M+1)^+$] confirms the successful synthesis of this intermediate.

2.2.3 Synthesis of 5-Methoxy-2,3,3-Trimethyl-N-Dimethyl-Octyl-Semisquaraine Ethyl-Ester[3]and its Hydrolyzed Product [4]

10 mmol of compound (2), 20 mmol of 3,4-diethoxy-3-cyclobutene-1,2-dione (3 mL) and 1 mL of triethylamine and ethanol (50 ml) were taken in a round bottom flask fitted with condenser. Reaction mixture was refluxed followed by progress monitoring with TLC and quenched after 8 hours leading to a greenish solution. Reaction mixture was concentrated over rotary evaporator and crude product was purified using ethyl acetate/hexane as the eluting solvent by flash column chromatography giving titled compound (3) in 50% yield as yellow solid. This semi-squaraine ester (3) was then subjected to hydrolysis using 40% NaOH in ethanol for 30 mins. The solvent was removed and HCl was added for neutralization. The compound was then extracted in ethyl acetate washing thoroughly with 10 % Na_2CO_3 aqueous solution. The extract was then concentrated to give orange solid. FAB-MS measured (426.40) and calculated (425.25) confirms the identity of synthesized product.

2.2.4 Synthesis of 5-Carboxy-2,3,3-Trimethyl-1-Dimethyl-Octyl-Indolium Iodide [5]

9.6 mmol of 5-Carboxy-2,3,3-trimethyl indole (2.0 g) was taken in a round bottom flask fitted with a condenser. 13.8 mmol of 3,7-dimethyl-1-octyl iodide and 40 mL in anhydrous acetonitrile were added to the round bottom flask and the reaction mixture was refluxed followed by monitoring of the reaction by thin layer chromatography (TLC). The reaction was completed in 48 hours. Solvent was evaporated under vacuum and ample diethyl ether was added for precipitation followed by filtration. The pinkish solid compound was obtained in 60% yield. FAB-MS (345.72) is well in accordance with the calculated mass of 345.26.

2.2.5 Synthesis of squaraine dye SQ-110

0.7 mmol (330 mg) of the intermediate (5) and hydrolysed semi-squaraine dye intermediate (4) were dissolved in 30 mL toluene/butanol (1:1) in a round bottom flask fitted with condenser. Reaction mixture was then refluxed for 18 hours followed by solvent removal with the aid of rotary evaporator. Crude dye was then subjected to flash column chromatography using $CHCl_3$/MeOH (9:1) as the eluting solvent giving titled dye SQ 110 as blue solid in 82% yield

> 98 % purity as confirmed by HPLC. High resolution FAB-MS measured 751.5012 $[M+1]^+$ and calculated (750.4972) and ^{1}H NMR (500 MHz, d6-DMSO): d/ppm = 7.95 (d, H-30), 7.92 (d, H-4), 7.34 (dd, H-6), 7.28 (d, H-27), 7.23 (dd, H-29), 6.95 (dd, H-7), 5.87 (s, H-10), 5.72 (s, H-23), 4.03 (t, 2H, H-13), 4.15 (t, 2H, H-35), 1.03 (s, 6H, H-11 & H-12), 1.13 (s, 6H, H-33 & H-34), 0.87 (m, 15H, H-20, H-21, H-22, H-42 & H-43) confirms the successful synthesis of this dye.

2.2.6 SYNTHESIS OF THE SQUARAINE DYE SQ-111

0.5 mmol (236 mg) of the intermediate (4) and hydrolyzed semi-squaraine dye intermediate (6) were dissolved in 30 mL toluene/butanol (1:1) in a round bottom flask fitted with condenser. Reaction mixture was then refluxed for 18 hours allowing condensation. After the completion of reaction as confirmed by TLC, the solvent was removed by rotary evaporator. The crude dye was then subjected to flash column chromatography using $CHCl_3$ / MeOH (9:1) as the eluting solvent. The isolated pure fraction was then concentrated to give a blue solid as titled dye in the 62% yield and >98 % purity. The measured HR-FAB-MS 721.3784 $[M+1]^+$ supported the synthesis of SQ 111 whose mass was obtained as 720.3790 theoretically. ^{1}H NMR (500 MHz, d6-DMSO): d/ppm = 7.93 (dd, H-24), 7.92 (d, H-4), 7.68 (d, H-6), 7.36 (d, H-21), 7.29 (d, H-23), 6.97 (dd, H-7), 5.88 (s, H-17), 5.76 (s, H-12), 4.18 (t, 2H, H-13), 4.07 (t, 2H, H-29), 1.71 (s, 6H, H-10 & H-11), 1.28 (s, 6H, H-27 & H-28), 0.87 (m, 9H, H-32, H-37, H-38). FB-MS and NMR data verifies the identity of the synthesized final dye SQ 111.

2.2.7 SYNTHESIS OF COBALT BIPYRIDYL COMPLEXES

2,2-bipyridyl (30 mmol) was dissolved in 25 mL methanol and stirred gently until dissolution. 1 eq. of $CoCl_2$ (10 mmol) was added to the above reaction mixture. It was then refluxed for 3 hours. 70% of the solvent was removed. Aqueous solution of NH_4PF_6 (31 mmol) was added to the above reaction mixture which resulted in a light yellow precipitate. The precipitate was filtered and washed thoroughly with methanol to give the $Co(bpy)_3(PF_6)_2$. 2 mmol of this

$Co(bpy)_3(PF_6)_2$. was dissolved in 20 mL acetonitrile followed by addition of 3 mmol of $NOBF_4$ for oxidation. This reaction mixture was stirred for 30 mins at room temperature. Excess of aqueous NH_4PF_6 (6 mmol) was then added for precipitation followed filtration to get the $Co(bpy)_3(PF_6)_3$ as bright yellow solid.

3. Results and Discussion

3.1 Optical Characterization

Electronic absorption of the four unsymmetrical squaraine dyes utilized for present investigation in both of the solution as well as on solid-state are shown in the Fig. 3. Parameters deduced from the electronic absorption spectral investigation are summarized in the table 1. It can be seen that these squaraine dyes exhibit light absorption mainly in the far-red region of the solar spectrum. This intense light absorption with molar extinction coefficients (□) varying from 1.8-2.4 $\times 10^5$ $dm^3mol^{-1}cm^{-1}$ in the 550 nm-700 nm wavelength region are associated with the π- π^* electronic transition from their highest occupied molecular orbital (HOMO) to lowest unoccupied molecular orbital (LUMO). A perusal of the Fig. 3(a) clearly corroborates that amongst unsymmetrical squaraine dyes under investigation, SQ-110 shows the highest bathochromically shifted light absorption with absorption maximum (λ_{max}) at 649 nm with a very high□□ of 2.4 $\times 10^5$ dm^3 mol^{-1} cm^{-1}. This bathochromic shift in the λ_{max} for both of the dyes SQ-110 and SQ-111 is due to the presence of electron donating $–OCH_3$ substituted at the 5^{th} position of the indole ring. However, SQ-110 and SQ-111 exhibit relatively pronounced vibronic shoulders around 600 nm though they bear two long alkyl chains as substituents. This could be associated with enhanced hydrogen bonding interactions between the dyes facilitated by methoxy group leading to dye aggregation. Intensification of this vibronic shoulder has been attributed to formation of H-aggregates by the dye molecules as reported previously [20].

In order to probe this observation more precisely solid-state electronic absorption spectra of dyes after their adsorption on mesoporous TiO_2 (Fig 3b) was also recorded. Solid-

state absorption spectra of the dyes taken on to the 3 μm thick mesoporous TiO_2 layer not only show further bathochromic shift in the λ_{max} but also the spectral broadening. This could be explained considering the interaction of the dye with TiO_2 via the ester linkage and the higher aggregation is due to more feasibility of aggregate formation in the close vicinity [21]. Planarity induced by extended π-conjugation in these dyes make them prone to dye-aggregation and it has been reported that dye aggregates (especially blue-shifted H-aggregates) are less prone to electron injection as compared to monomeric dye leading to hampered photon harvesting in the solar cells [22]. This is the reason why utilization of dye-aggregating agent CDCA with sensitizing play a vital role for efficient photon harvesting in DSSCs by controlling the dye aggregation [23, 24].

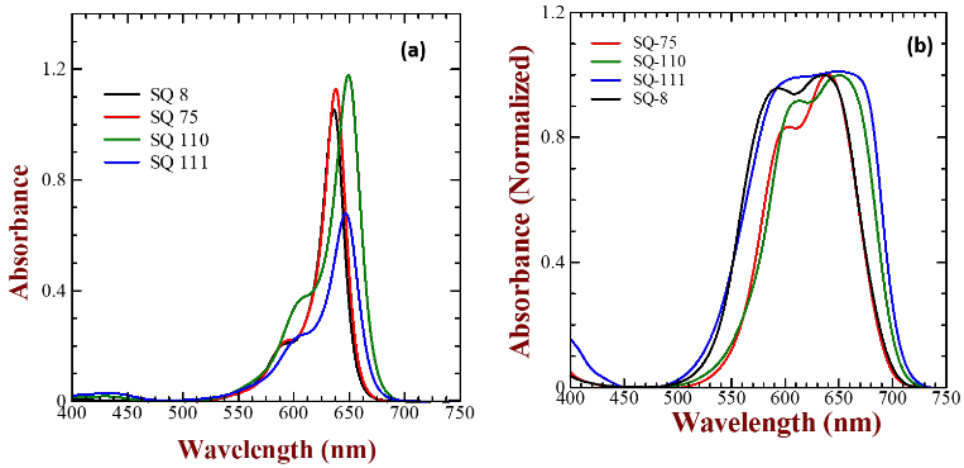

Figure 3. Electronic absorption spectra of the unsymmetrical squaraine dyes in ethanol (5□M) (a) and normalized absorption spectra in solid-state for the same dyes adsorbed on 3μm thick transparent TiO_2 (b).

Normalized solid-state electronic absorption spectrum of the dyes on TiO_2 (Fig. 3b) indicates a pronounced blue-shifted vibronic shoulder around 610 nm as compared to that in solution associated with H-aggregate formation. Therefore, ratio between absorbance of the H-aggregate band (around 610 nm) and the monomer band in solution (650) can be used as indicator of extent of H-aggregation, which has also been summarized in the table 1. It is worth to mention here that, while recording solid-state electronic absorption spectrum of dyes, no

CDCA has been used in the solution in order to precise probing of the structure property correlation. In an interesting work, Yum et al. reported that extent of H-aggregates of squaraine dye on the mesoporous TiO_2 decreases as function of added fraction of bulky CDCA in dye solution as co-adsorber, which prevents the dye aggregation [20]. A perusal of Fig 3(b) and table 1 clearly corroborates that as compared solution, there is pronounced H-aggregate formation in the solid-state owing to enhanced intermolecular interaction. Higher extent of aggregation for SQ-8 (0.96) as compared to that of SQ-75 (0.84) could be associated with presence of short alkyl chain (ethyl) which is unable to hinder the dye aggregation. On the other hand, higher extent of dye aggregation in spite of the presence of long alkyl chains for the sensitizing dyes SQ-110 and SQ-111 could be attributed to enhanced intermolecular hydrogen bonding due to presence of direct ring substituted methoxy group and terminal –F substitution in the alkyl chains.

3.2 Energy Band Diagram

Apart from high molar extinction coefficient and presence of suitable anchoring group, sensitizing dyes must exhibit energetic cascade with respect to the wide band gap semiconductor (TiO_2) in this work) and redox electrolyte under investigation. Energy of their highest occupied molecular orbital (HOMO) and lowest unoccupied molecular orbital (LUMO) should be lower than the redox energy level of the electrolyte and conduction band energy level of TiO_2 for the dye regeneration and electron injection, respectively [25]. HOMO energy level of the sensitizing dyes was calculated by photoelectron yield spectroscopy (PYS) under vacuum (10^{-3} Pascal). On the other hand, energy of the LUMO was estimated by adding energy corresponding the optical band gap (Eg) to their respective HOMO energy value. Eg for the sensitizing dyes was estimated from the offset of the solid-state electronic absorption spectra of the respective dyes shown in the Fig. 3(b). Energy band diagram thus constructed for sensitizers used in this work along with the TiO2 and cobalt based redox electrolyte is shown

in the Fig. 4. As illustrated by Fig. 4 that all of the far-red sensitive unsymmetrical squaraine dyes have their LUMO energy above the CB of the TiO_2, which is considered to be 4 eV lower than the vacuum level [26]. This ensures the electron injection from the excited dye molecules to the TiO_2 after the photoexcitation.

Table 1. Optical and energetic parameters of the unsymmetrical squaraine dyes extracted from the photophysical investigations.

Dye	λ_{max} solution	ϵ in solution ($dm^3.mol^{-1}.cm^{-1}$)	λ_{max} solid-state	Aggregation on TiO_2	HOMO (eV)	LUMO (eV)
SQ-8	637 nm	2.08×10^5	638 nm	0.96	-5.15	-3.33
SQ-75	638 nm	2.24×10^5	640 nm	0.84	-5.05	-3.37
SQ-110	649 nm	2.34×10^5	652 nm	0.92	-5.10	-3.22
SQ-111	648 nm	1.75×10^5	652 nm	0.99	-5.20	-3.40

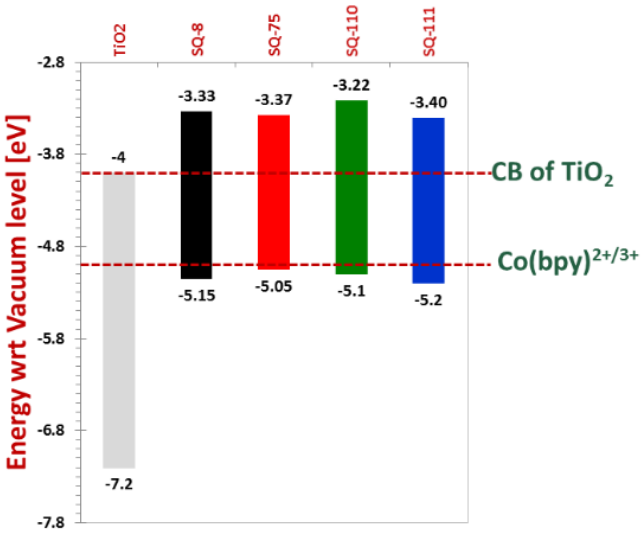

Figure 4. Energy band diagram representing energy level of sensitizing dyes, cobalt complex electrolyte and wide band gap semiconductor (TiO_2).

It can be further seen that amongst the four sensitizers, SQ-110 depicts the highest LUMO energy level and thus provide the largest driving force for the electron injection with an energy barrier of 0.67 eV. SQ-110 and SQ-75 bear long alkyl chains with electron donating tendency, which as a result raises the energy level as compared to that of SQ-8 [18]. The upward shift in

the HOMO energy level of SQ-110 could also be due to the presence of the electron donating $–OCH_3$ group on the 5^{th} position of the indole ring. However, SQ-111 differs from SQ-110 only with the N substitution, where former bears the electron donating dimethyl octyl group whereas the latter bears the electron withdrawing trifluoro substituent (negative inductive effect). The effect of the electron-withdrawing group in the energetics is vividly shown by the downward shift in both of the HOMO and LUMO of SQ-111 as compared to that of SQ-110. It is interesting to note that SQ-75 bearing only one long alkyl chain exhibits highest HOMO energy level of -5.05 eV amongst dyes used, which is very near to redox potential of the cobalt bipyridyl complex based electrolyte (-5.00 eV). Although there is a very small energy barrier (0.05 eV) between the HOMO of SQ-75 and redox energy level of Cobalt electrolyte, still there is regeneration of the dye as evidenced by photon harvesting discussed in the next section.

3.3 Photovoltaic Characterization

Energetic match of all of the sensitizers used under present investigation with respect to TiO2 as wide band gap semiconductor and Co(bpy)2+/3+ redox electrolyte along with their higher molar extinction coefficient encourage us to explore their potentiality as sensitizer for DSSC application. DSSCs were fabricated under identical experimental conditions like fabrication of photoelectrode, concentration of dye/CDCA and cobalt redox electrolyte only by changing the sensitizers such as SQ-8, SQ-75, SQ-110 and SQ-111. Photovoltaic characteristics of the DSSCs thus under simulated solar irradiation have been shown in the Fig. 5 along with summarized photovoltaic parameters shown the table 2. It can be seen from the Fig. 5 that SQ-110 bearing two long alkyl group exhibited the best photoconversion efficiency (PCE) of 1.98 % having the highest short-circuit current density (Jsc) of 5.9 mA/cm2 and open-circuit voltage (Voc) of 0.57 V after simulated 1-Sun solar irradiation.

From the device point of view, this improved photovoltaic performance for the DSSC based on SQ-110 could be attributed to the facile electron injection in TiO_2 and reduced charge recombination. Another plausible explanation for the best performance of the DSSC using SQ-110 could be given to the molecular structure this dye. Two branched and long alkyl chains consisted of dimethyloctyl function well as an effective blocking layer for the charge recombination minimizing voltage loss. At the same time, the highest lying LUMO energy level of this dye provides relatively better driving force for electron injection from the photoexcited dye to the CB of TiO_2. It can also be seen that hampered photovoltaic performance with PCE of (1.24 %) was exhibited by the dye SQ-8, bearing only short alkyl chain (ethyl). DSSCs using mesoporous TiO_2 and cobalt redox shuttles are more prone to charge recombination and demands for the strict surface passivation. This surface passivation has been reported to be accomplished not only by using compact oxide thin layer but also by utilization of dyes having long alkyl chains to provide additional effective surface passivation of the mesoporous TiO_2 [27,28,29,30,]. It has also been reported that sensitizing dyes bearing long alkyl chains are preferred choice for DSSCs using cobalt-based redox electrolyte, which acts a barrier for back electron transfer from the injected electrons of TiO_2 and positively charged $Co(bpy)^{2+/3+}$ ions in the electrolyte [31]. We would like to emphasize here that we have previously attempted SQ-8 as sensitizer for DSSC using cobalt redox electrolytes but efficiency was very low (0.2-0.3 %) [16]. Such a seriously hampered PCE for SQ-8 in our previous report could be attributed to lack of surface passivation of FTO and mesoporous TiO_2, which led to pronounced enhancement in the PCE up 1.23 % after surface passivation in this work. At the same, lack of long alkyl chain in SQ-8 is responsible for its relatively hampered PCE as compared to the SQ-110 bearing very long alkyl substituent in the dye molecular framework.

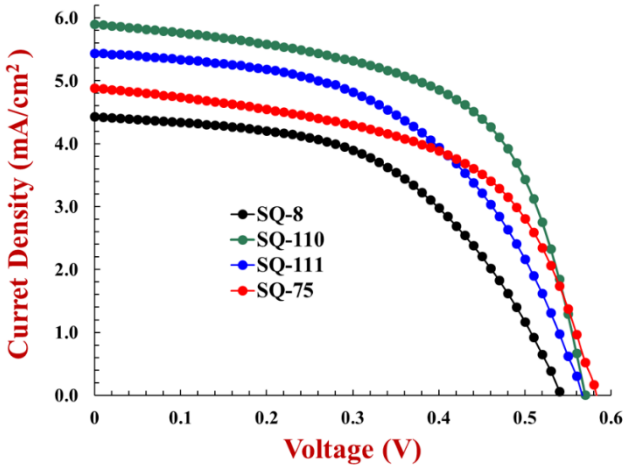

Figure 6. Photovoltaic characteristics of DSSCs under simulated 1-Sun irradiation fabricated using different sensitizers and cobalt redox electrolyte.

Table 2. Photovoltaic parameters extracted from photovoltaic characteristics for the DSSCs fabricated using different sensitizers and cobalt redox electrolyte.

Dye	Jsc (mA/cm^2)	Voc (V)	FF	Efficiency (%)
SQ-8	4.43	0.54	0.52	1.24
SQ-75	4.88	0.58	0.56	1.58
SQ-110	5.90	0.57	0.59	1.98
SQ-111	5.44	0.56	0.51	1.58

Importance and need of driving force for electron injection and dye regeneration has been well documented in the DSSC research and there is a consensus that higher driving force promotes them [32,33]. A perusal of the energetics from the Fig. 4 clearly indicates that although SQ-75 exhibits lower LUMO and higher HOMO energy as compared to that of SQ-8, however it shows higher Jsc of 4.88 mA/cm^2 and Voc of 0.58 V (table-2) as compared to that of SQ-8. This also signifies the implication of the screening effect of very long alkyl chain (dodecyl) on the charge recombination, which is absent in SQ-8. Obtained photovoltaic parameters for all of the dyes clearly show the importance of long alkyl chains for making them compatible to cobalt electrolytes. SQ-111 based DSSCs exhibited hampered PCE (1.58 %) compared to that of SQ-110 in spite of relatively deeper HOMO energy level. This could be

attributed to hampered electron injection due to enhanced dye aggregation (H-aggregates, table-1) leading to increased charge recombination. It has also been reported that as compared to monomeric dye molecules, dye aggregates exhibit lower efficiency of charge injection leading to hampered Jsc (table-2) [34]. Therefore, this is also the clear indication that dye molecular structure plays rather crucial role in our case as compared to its energy levels in controlling the overall photovoltaic performance of the DSSC.

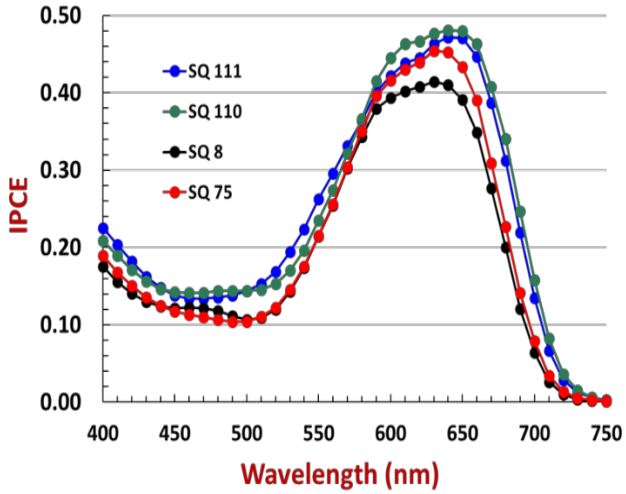

Figure 7. Photocurrent action spectra for DSSCs fabricated using different sensitizers and cobalt redox electrolyte after monochromatic illumination.

Photocurrent action spectra has been widely used in solar cell research in order to independently verify the observed photovoltaic characteristics in general and Jsc in particular. It is the plot of incident photon to electron conversion efficiency (IPCE) as a function of wavelength of incident photons. Photocurrent action spectra of DSSCs fabricated using various unsymmetrical squaraine dyes and cobalt redox electrolyte have been shown in the Fig. 7. A resemblance between the photocurrent action spectrum and solid-state electronic absorption spectrum (Fig. 3b) of the sensitizer ascertains that photocurrent is generated by the electron injection from the excited dye molecule to the conduction band of TiO_2 after photo excitation.

It can be clearly seen from the Fig. 6 and table-2 that the peak of IPCE follows the same trend of Jsc values for the respective sensitizers. At the same time, SQ-110 exhibits an IPCE of 48 % at 650 nm, which is higher as compared to that of SQ-8 (41 % at 640 nm) and justifies the higher Jsc value for the DSSC made with dye SQ-110. Presence of electronic donating methoxy group in the sensitizers SQ-110 and SQ-111 led to the bathochromically shifted $\square_{max}$ and optical absorption edge (Fig. 3b) which has also been well reflected in the photon harvesting behavior by the DSSC fabricated using dyes. In spite of having lowest driving force of only 0.05 eV (Fig. 4) for dye regeneration with $Co(bpy)^{2+/3+}$ electrolyte, SQ-75 exhibits appreciably good photon harvesting in the far-red wavelength region. This indicates about the possibility design and development of novel sensitizing dyes and cobalt complexes with deeper HOMO and redox energy level, respectively for NIR photon harvesting.

Conclusions

A series of far-red sensitive unsymmetrical squaraine dyes were successfully synthesized followed by their photophysical characterizations and application as sensitizer for DSSC based on cobalt redox shuttle. Logical molecular design led to the photon harvesting mainly in the far-red wavelength region with onset extending up to 750 nm. All of the blue coloured squaraine dyes employed in the work, worked well as sensitizer for DSSC utilizing cobalt complex based redox electrolyte. However, it was found that the molecular structure of the dyes plays rather more important role than the energetics in determining the overall performance of the DSSCs. It was well proven that long alkyl chains screen the TiO_2 from the direct contact between the cobalt ions of the electrolyte and TiO_2 surface and impede the charge recombination. It was demonstrated that DSSC based on one of the newly designed sensitizer SQ-110 bearing two long alkyl chains exhibited the best PCE of about 2 % with photon harvesting extending up to 750 nm in the NIR region.

REFERENCES

1. O'Regan, B.; Grätzel, M., A low-cost, high-efficiency solar cell based on dye-sensitized colloidal TiO2 films. *Nature* **1991,** *353* (6346), 737.
2. Grätzel, M., Conversion of sunlight to electric power by nanocrystalline dye-sensitized solar cells. *Journal of Photochemistry and Photobiology A: Chemistry* **2004,** *164* (1-3), 3-14.
3. Tachibana, Y.; Moser, J. E.; Grätzel, M.; Klug, D. R.; Durrant, J. R., Sub picosecond interfacial charge separation in dye-sensitized nanocrystalline titanium dioxide films. *The Journal of Physical Chemistry* **1996,** *100* (51), 20056-20062.
4. Salvatori, P.; Marotta, G.; Cinti, A.; Anselmi, C.; Mosconi, E.; De Angelis, F., Supramolecular interactions of chenodeoxycholic acid increase the efficiency of dye-sensitized solar cells based on a cobalt electrolyte. *The Journal of Physical Chemistry C* **2013,** *117* (8), 3874-3887.
5. Yella, A.; Mai, C. L.; Zakeeruddin, S. M.; Chang, S. N.; Hsieh, C. H.; Yeh, C. Y.; Grätzel, M., Molecular engineering of push–pull porphyrin dyes for highly efficient dye-sensitized solar cells: The role of benzene spacers. *Angewandte Chemie* **2014,** *126* (11), 3017-3021.
6. Higashino, T.; Imahori, H., Porphyrins as excellent dyes for dye-sensitized solar cells: recent developments and insights. *Dalton Transactions* **2015,** *44* (2), 448-463.
7. Pandey, S. S.; Watanabe, R.; Fujikawa, N.; Shivashimpi, G. M.; Ogomi, Y.; Yamaguchi, Y.; Hayase, S., Effect of extended π-conjugation on photovoltaic performance of dye sensitized solar cells based on unsymmetrical squaraine dyes. *Tetrahedron* **2013,** *69* (12), 2633-2639.
8. Hardin, B. E.; Snaith, H. J.; McGehee, M. D., The renaissance of dye-sensitized solar cells. *Nature photonics* **2012,** *6* (3), 162.
9. Hamann, T. W.; Jensen, R. A.; Martinson, A. B.; Van Ryswyk, H.; Hupp, J. T., Advancing beyond current generation dye-sensitized solar cells. *Energy & Environmental Science* **2008,** *1* (1), 66-78.
10. Cheng, M.; Yang, X.; Li, S.; Wang, X.; Sun, L., Efficient dye-sensitized solar cells based on an iodine-free electrolyte using l-cysteine/l-cystine as a redox couple. *Energy & Environmental Science* **2012,** *5* (4), 6290-6293.
11. Mosconi, E.; Yum, J.-H.; Kessler, F.; Gómez García, C. J.; Zuccaccia, C.; Cinti, A.; Nazeeruddin, M. K.; Grätzel, M.; De Angelis, F., Cobalt electrolyte/dye interactions in dye-sensitized solar cells: a combined computational and experimental study. *Journal of the American Chemical Society* **2012,** *134* (47), 19438-19453.
12. Feldt, S. M.; Gibson, E. A.; Gabrielsson, E.; Sun, L.; Boschloo, G.; Hagfeldt, A., Design of organic dyes and cobalt polypyridine redox mediators for high-efficiency dye-sensitized solar cells. *Journal of the American Chemical Society* **2010,** *132* (46), 16714-16724.
13. Yang, J.; Ganesan, P.; Teuscher, J. l.; Moehl, T.; Kim, Y. J.; Yi, C.; Comte, P.; Pei, K.; Holcombe, T. W.; Nazeeruddin, M. K., Influence of the donor size in D− π–A organic dyes for dye-sensitized solar cells. *Journal of the American Chemical Society* **2014,** *136* (15), 5722-5730.
14. Tsao, H. N.; Yi, C.; Moehl, T.; Yum, J. H.; Zakeeruddin, S. M.; Nazeeruddin, M. K.; Grätzel, M., Cyclopentadithiophene Bridged Donor–Acceptor Dyes Achieve High Power Conversion Efficiencies in Dye-Sensitized Solar Cells Based on the tris- Cobalt Bipyridine Redox Couple. *ChemSusChem* **2011,** *4* (5), 591-594.
15. Hao, Y.; Saygili, Y.; Cong, J.; Eriksson, A.; Yang, W.; Zhang, J.; Polanski, E.; Nonomura, K.; Zakeeruddin, S. M.; Grätzel, M., Novel blue organic dye for dye-sensitized solar cells achieving high efficiency in cobalt-based electrolytes and by co-sensitization. *ACS applied materials & interfaces* **2016,** *8* (48), 32797-32804.
16. Marchena, M. J.; de Miguel, G.; Cohen, B.; Organero, J. A.; Pandey, S.; Hayase, S.; Douhal, A., Real-time photodynamics of squaraine-based dye-sensitized solar cells with iodide and cobalt electrolytes. *The Journal of Physical Chemistry C* **2013,** *117* (23), 11906-11919.

17. Pradhan, A.; Morimoto, T.; Saikiran, M.; Kapil, G.; Hayase, S.; Pandey, S. S., Investigation of the minimum driving force for dye regeneration utilizing model squaraine dyes for dye-sensitized solar cells. *Journal of Materials Chemistry A* **2017,** *5* (43), 22672-22682.
18. Pandey, S. S.; Inoue, T.; Fujikawa, N.; Yamaguchi, Y.; Hayase, S., Substituent effect in direct ring functionalized squaraine dyes on near infra-red sensitization of nanocrystalline TiO2 for molecular photovoltaics. *Journal of Photochemistry and Photobiology A: Chemistry* **2010,** *214* (2-3), 269-275.
19. Pandey, S. S.; Inoue, T.; Fujikawa, N.; Yamaguchi, Y.; Hayase, S., Alkyl and fluoro-alkyl substituted squaraine dyes: A prospective approach towards development of novel NIR sensitizers. *Thin Solid Films* **2010,** *519* (3), 1066-1071.
20. Yum, J.; Moon, S.; Humphry-Baker, R.; Walter, P.; Geiger, T.; Nüesch, F.; Grätzel, M.; d K Nazeeruddin, M., Effect of coadsorbent on the photovoltaic performance of squaraine sensitized nanocrystalline solar cells. *Nanotechnology* **2008,** *19* (42), 424005.
21. Yum, J.-H.; Walter, P.; Huber, S.; Rentsch, D.; Geiger, T.; Nüesch, F.; De Angelis, F.; Grätzel, M.; Nazeeruddin, M. K., Efficient far red sensitization of nanocrystalline TiO2 films by an unsymmetrical squaraine dye. *Journal of the American Chemical Society* **2007,** *129* (34), 10320-10321.
22. Zhang, L.; Cole, J. M., Dye aggregation in dye-sensitized solar cells. *Journal of Materials Chemistry A* **2017,** *5* (37), 19541-19559.
23. Pradhan, A.; Saikiran, M.; Kapil, G.; Pandey, S. S.; Hayase, S. In *Parametric Optimization of Dye-Sensitized Solar Cells Using Far red Sensitizing Dye with Cobalt Electrolyte*, Journal of Physics: Conference Series, IOP Publishing: 2017; p 012001.
24. Kang, X.; Zhang, J.; O'Neil, D.; Rojas, A. J.; Chen, W.; Szymanski, P.; Marder, S. R.; El-Sayed, M. A., Effect of molecular structure perturbations on the performance of the D–A− π–A dye sensitized solar cells. *Chemistry of Materials* **2014,** *26* (15), 4486-4493.
25. Ananthakumar, S.; Ramkumar, J.; Babu, S. M., Semiconductor nanoparticles sensitized TiO2 nanotubes for high efficiency solar cell devices. *Renewable and Sustainable Energy Reviews* **2016,** *57*, 1307-1321.
26. Lenzmann, F.; Krueger, J.; Burnside, S.; Brooks, K.; Grätzel, M.; Gal, D.; Rühle, S.; Cahen, D., Surface photovoltage spectroscopy of dye-sensitized solar cells with TiO2, Nb2O5, and SrTiO3 nanocrystalline photoanodes: indication for electron injection from higher excited dye states. *The Journal of Physical Chemistry B* **2001,** *105* (27), 6347-6352.
27. Chai, Q.; Li, W.; Wu, Y.; Pei, K.; Liu, J.; Geng, Z.; Tian, H.; Zhu, W., Effect of a Long Alkyl Group on Cyclopentadithiophene as a Conjugated Bridge for D–A− π–A Organic Sensitizers: IPCE, Electron Diffusion Length, and Charge Recombination. *ACS applied materials & interfaces* **2014,** *6* (16), 14621-14630.
28. DeVries, M. J.; Pellin, M. J.; Hupp, J. T., Dye-sensitized solar cells: driving-force effects on electron recombination dynamics with cobalt-based shuttles. *Langmuir* **2010,** *26* (11), 9082-9087.
29. Kay, A.; Grätzel, M., Dye-sensitized core− shell nanocrystals: improved efficiency of mesoporous tin oxide electrodes coated with a thin layer of an insulating oxide. *Chemistry of Materials* **2002,** *14* (7), 2930-2935.
30. Cui, Y.; Wu, Y.; Lu, X.; Zhang, X.; Zhou, G.; Miapeh, F. B.; Zhu, W.; Wang, Z.-S., Incorporating benzotriazole moiety to construct D–A− π–A organic sensitizers for solar cells: significant enhancement of open-circuit photovoltage with long alkyl group. *Chemistry of Materials* **2011,** *23* (19), 4394-4401.
31. Qu, S.; Wu, W.; Hua, J.; Kong, C.; Long, Y.; Tian, H., New diketopyrrolopyrrole (DPP) dyes for efficient dye-sensitized solar cells. *The Journal of Physical Chemistry C* **2009,** *114* (2), 1343-1349.

32. Feldt, S. M.; Wang, G.; Boschloo, G.; Hagfeldt, A., Effects of driving forces for recombination and regeneration on the photovoltaic performance of dye-sensitized solar cells using cobalt polypyridine redox couples. *The Journal of Physical Chemistry C* **2011,** *115* (43), 21500-21507.
33. Daeneke, T.; Mozer, A. J.; Uemura, Y.; Makuta, S.; Fekete, M.; Tachibana, Y.; Koumura, N.; Bach, U.; Spiccia, L., Dye regeneration kinetics in dye-sensitized solar cells. *Journal of the American Chemical Society* **2012,** *134* (41), 16925-16928.
34. Khazraji, A. C.; Hotchandani, S.; Das, S.; Kamat, P. V., Controlling dye (merocyanine-540) aggregation on nanostructured TiO2 films. An organized assembly approach for enhancing the efficiency of photosensitization. *The Journal of Physical Chemistry B* **1999,** *103* (22), 4693-4700.

Graphical Abstract